A dam-break flood simulation model in curvilinear coordinates

GIOVANNI CANNATA, CHIARA PETRELLI, LUCA BARSI, FEDERICO FRATELLO, FRANCESCO GALLERANO
Department of Civil, Constructional and Environmental Engineering
Sapienza University of Rome
Via Eudossiana 18, 00184 Rome, Italy
ITALY
giovanni.cannata@uniroma1.it https://www.dicea.uniroma1.it/en/users/giovannicannata

Abstract: - A dam-break flood model based on a contravariant integral form of the shallow water equations is presented. The numerical integration of the equations of motion is carried out by means of a finite volume-finite difference numerical scheme that involves an exact Riemann solver and which is based on a high-order WENO reconstruction procedure. An original scheme for the simulation of the wet front progress on the dry bed is adopted. The proposed model capacity to correctly simulate the wet front progress velocity is tested by numerically reproducing the dry bed dam-break problem. The model is adopted for the real case study of the Rio Fucino lake-dam collapse and subsequent flood wave propagation, downstream of the Campotosto reservoir (Italy).

Key-Words: - shallow water equations, curvilinear coordinates, shock-capturing, dam-break flood, exact Riemann solver, wet and dry front

1 Introduction

Rio Fucino dam is a concrete lake-dam that functions as a barrier to the Campotosto reservoir (Italy), which is among the largest artificial basin in Europe. The reservoir is located in the natural reserve of Monti della Laga at 1313m of altitude, has a surface of 14km^2 and a water volume of 300million m^3 with 35m maximum depth.

In the context of the safety assessment of the existing Italian dams, the Rio Fucino dam is of particular interest as it is very close to the Monti della Laga seismic fault. This fault, about 30km long, is parallel to the dam body and its track is distant about 300m from it. The Monti della Laga fault may produce seismic events of magnitude greater than or equal to 7 and has caused the earthquakes that have led to the destruction of L'Aquila (6 April 2009) and Amatrice (24 August 2016). Following these seismic events, more attention has been paid to the Rio Fucino dam and to the side effects to which the potential interaction with the fault can lead to. In fact, the short distance of the Monti della Laga fault from the foundation of the dam compared to the size of the fault, does not preclude the foundations of the dam to be affected by the activity of the fault. In the event of fault breakage at the surface of the earth, the possible damages and the possible breaking of the aforementioned Rio Fucino dam would cause flood wave propagation along the Rio Fucino River and the Vomano valley. On the basis of such considerations, it is clear the need to simulate the Rio Fucino dam-break and subsequent flood wave propagation.

The flood maps that have been produced several decades ago, have been realized by using one-dimensional numerical schemes that approximate the unsteady flow, which takes place downstream of the dam, as a succession of steady flows. This simplification carries out a qualitative assessment of the outflow flow and of the trend over time of the flow produced by the flood wave.

In the most recent literature [3][10][13-15], there are methods able to directly simulate the propagation of the discontinuity by means of shock-capturing schemes based on the two-dimensional depth-averaged shallow water equations. Furthermore, in order to simulate the overflow phenomenon over computational domains reproducing the river channel complex morphology, it is possible to adopt a strategy that numerically integrates the equations of motion on generalized curvilinear boundary-conforming grids. By using boundary-conforming curvilinear coordinates, the equations of motion can be written in contravariant formulation [1-2][4].

In this work we present the study of the flood wave propagation downstream of the Rio Fucino dam due to the dam-break and subsequent emptying of the Campotosto reservoir, in the case of initial full supply water level. The equations of motion are

numerically solved by means of a finite volume numerical scheme that involves an exact Riemann solver and is based on a high-order WENO reconstruction procedure [5][7]. For the simulation of the wet front progress on the dry bed, an original wet and dry scheme is used. The capacity of the proposed model to correctly simulate the wet front progress velocity is tested by numerically reproducing the dam-break problem on a dry bed.

2 Problem Formulation

The model is based on the integral contravariant formulation of the two dimensional shallow water equations.

Let $\vec{v} = \vec{u}h$ where h and $\vec{u}$ are, respectively, the water depth and the depth-averaged velocity vector whose components are defined in the Cartesian system of reference.

We consider the coordinate transformation $x^l = x^l(\xi^1, \xi^2)$ from the Cartesian coordinate system $\vec{x}$ to the curvilinear coordinate system $\vec{\xi}$ (note that superscripts indicate the generic component and not powers). Let $\vec{g}_{(l)} = \partial\vec{x}/\partial\xi^l$ be the covariant base vectors and $\vec{g}^{(l)} = \partial\xi^l/\partial\vec{x}$ the contravariant base vectors. The covariant and contravariant metric coefficients are given respectively by $g_{lm} = \vec{g}_{(l)} \cdot \vec{g}_{(m)}$ and $g^{lm} = \vec{g}^{(l)} \cdot \vec{g}^{(m)}$. The Jacobian of the transformation is given by $\sqrt{g} = \sqrt{|g_{lm}|}$ where $|\ \ |$ denotes the determinant of the covariant metric coefficients g_{lm}. The transformation relationships between vector $\vec{v}$ in the Cartesian coordinate system and its contravariant, v^l, and covariant, v_l, components in the curvilinear coordinate system are given by

$$v^l = \vec{g}_{(l)} \cdot \vec{v} \quad ; \quad \vec{v} = v^l \vec{g}_{(l)}$$

$$v_l = \vec{g}_{(l)} \cdot \vec{v} \quad ; \quad \vec{v} = v_l \vec{g}^{(l)} \tag{1}$$

The shallow water equations in contravariant formulation read

$$\frac{\partial h}{\partial t} + v^l_{,l} = 0 \tag{2}$$

$$\frac{\partial v^l}{\partial t} + \left(\frac{v^l v^m}{h} + G\, g^{lm}\frac{h^2}{2}\right)_{,m} = -Gh\, g^{lm} H_{,m} - R^l \tag{3}$$

where a comma with an index in a subscript stands for covariant differentiation, the second term on the left-hand side of both equation (2) and (3) is the flux term, G is the constant of gravity, $-Gh\, g^{lm} H_{,m}$ is the source term related to the bottom slope in which H is the bottom elevation and R^l is the bottom resistance term.

The motion equations (2) and (3) are integrated over an arbitrary surface element of area ΔA, whose contour line is L, and are solved in the direction in space of a parallel vector field, $\lambda_k(\xi^1, \xi^2) = \vec{g}^{(l)} \cdot \vec{g}_{(k)}$, which is normal to the coordinate line on which the coordinate line ξ^l is constant. By recalling that by definition $\lambda_{k,m} = 0$ and that $\vec{g}_{(k)} \cdot \vec{g}^{(m)} = \delta^m_k$, the integral expressions of the shallow water equations in contravariant formulation are

$$\iint_{\Delta A} \frac{\partial h}{\partial t} dA + \int_L v^l n_m dL = 0 \tag{4}$$

$$\begin{aligned} &\iint_{\Delta A} \vec{\tilde{g}}^{(l)} \cdot \vec{g}_{(k)} \frac{\partial v^k}{\partial t} dA + \\ &\int_L \left(\vec{\tilde{g}}^{(l)} \cdot \vec{g}_{(k)} \frac{v^l v^m}{h} + \vec{\tilde{g}}^{(l)} \cdot \vec{g}^{(m)} G \frac{h^2}{2}\right) n_m dL \\ &= -\iint_{\Delta A} \vec{\tilde{g}}^{(l)} \cdot \vec{g}_{(k)} \left[Gh\, g^{km} H_{,m} + R^k\right] dA \end{aligned} \tag{5}$$

A restrictive condition on the surface element of area ΔA is now introduced: the surface element of area ΔA must be considered as a surface element which is bounded by four curves lying on the coordinate lines. Since $dA = \sqrt{g} d\xi^1 d\xi^2$ and by indicating the averaged values of h and v^l over the surface element of area ΔA as $\tilde{\bar{h}} = \frac{1}{\Delta A}\iint_{\Delta A} h\sqrt{g} d\xi^1 d\xi^2$ and $\tilde{\bar{v}}^l = \frac{1}{\Delta A}\iint_{\Delta A} \vec{\tilde{g}}^{(l)} \cdot \vec{g}_{(k)} v^k \sqrt{g} d\xi^1 d\xi^2$, equations (4) and (5) are rewritten as

$$\begin{aligned} &\frac{\partial \tilde{\bar{h}}}{\partial t} = \\ &-\frac{1}{\Delta A}\sum_{\alpha=1}^{2}\left[\int_{\Delta\xi^{\alpha+}} v^\alpha \sqrt{g} d\xi^\beta - \int_{\Delta\xi^{\alpha-}} v^\alpha \sqrt{g} d\xi^\beta\right] \end{aligned} \tag{6}$$

$$\begin{aligned} &\frac{\partial \tilde{\bar{v}}^l}{\partial t} = \frac{1}{\Delta A}\{-\sum_{\alpha=1}^{2} \\ &\left[\int_{\Delta\xi^{\alpha+}} \left(\vec{\tilde{g}}^{(l)} \cdot \vec{g}_{(k)} \frac{v^k v^\alpha}{h} + \vec{\tilde{g}}^{(l)} \cdot \vec{g}^{(\alpha)} G \frac{h^2}{2}\right)\sqrt{g} d\xi^\beta - \right. \\ &\left. \int_{\Delta\xi^{\alpha-}} \left(\vec{\tilde{g}}^{(l)} \cdot \vec{g}_{(k)} \frac{v^k v^\alpha}{h} + \vec{\tilde{g}}^{(l)} \cdot \vec{g}^{(\alpha)} G \frac{h^2}{2}\right)\sqrt{g} d\xi^\beta\right] \\ &- \iint_{\Delta A} \vec{\tilde{g}}^{(l)} \cdot \vec{g}_{(k)} \left[G(\eta - \tilde{\bar{\eta}})\, g^{km} H_{,m} + R^k\right] dA \\ &-G\tilde{\bar{\eta}} \sum_{\alpha=1}^{2}\left[\int_{\Delta\xi^{\alpha+}} \vec{\tilde{g}}^{(l)} \cdot \vec{g}_{(k)} H\sqrt{g} d\xi^\beta - \right. \\ &\qquad \left. \int_{\Delta\xi^{\alpha-}} \vec{\tilde{g}}^{(l)} \cdot \vec{g}_{(k)} H\sqrt{g} d\xi^\beta\right] \\ &+\frac{G}{2}\sum_{\alpha=1}^{2}\left[\int_{\Delta\xi^{\alpha+}} \vec{\tilde{g}}^{(l)} \cdot \vec{g}_{(k)} H^2\sqrt{g} d\xi^\beta - \right. \\ &\qquad \left. \int_{\Delta\xi^{\alpha-}} \vec{\tilde{g}}^{(l)} \cdot \vec{g}_{(k)} H^2\sqrt{g} d\xi^\beta\right\} \end{aligned} \tag{7}$$

in which the Christoffel symbols are absent. $\Delta\xi^{\alpha+}$ and $\Delta\xi^{\alpha-}$ indicate the segments of the contour line on which ξ^{α} is constant and which are located respectively at the larger and smaller value of ξ^{α} (α and β cyclic), $\eta = H + h$ is the free surface elevation and $\tilde{\bar{\eta}}$ represents the averaged value of η on the surface element ΔA. The last three terms on the right-hand side of equation (7) are obtained by decomposing the source term related to the bottom slope on the right-hand side of equation (5) as proposed by [16].

3 Problem Solution

The numerical integration of the equations of motion (6) and (7) is carried out by a high order upwind WENO (weighted essentially non-oscillatory) scheme. The computational domain discretization is based on a grid defined by the coordinate lines ξ^1 and ξ^2 and by the points of coordinates $\xi_i^1 = i\Delta\xi^1$ and $\xi_j^2 = j\Delta\xi^2$, which represent the centers of the calculation cells $I_{i;j} = \left(\xi_{i-1/2}^1,\ \xi_{i+1/2}^1\right) \times \left(\xi_{j-1/2}^2,\ \xi_{j+1/2}^2\right)$. t^n is the time level of the known variables, while $t^{n+1} = t^n + \Delta t$ is the time level of the unknown variables. Let us indicate with $\boldsymbol{L}(v^1, v^2)$ the right-hand side of equation (6) and with $\boldsymbol{D}(h,\ v^1, v^2)$ the right-hand side of equation (7). By integrating equations (6) and (7) over $[t^n, t^{n+1}]$ we get

$$\tilde{\bar{h}}_{i;j}^{(n+1)} = \tilde{\bar{h}}_{i;j}^{(n)} - \frac{1}{\Delta A}\int_{t^n}^{t^{n+1}} \boldsymbol{L}(v^1, v^2)dt \qquad (8)$$

$$\tilde{\bar{v}}^{l}{}_{i;j}^{(n+1)} = \tilde{\bar{v}}^{l}{}_{i;j}^{(n)} - \frac{1}{\Delta A}\int_{t^n}^{t^{n+1}} \boldsymbol{D}(h,\ v^1, v^2)dt \qquad (9)$$

Equations (8) and (9) represent the advancing from time level t^n to time level t^{n+1} of the variables $\tilde{\bar{h}}_{i;j}$ and $\tilde{\bar{v}}_{i;j}^{l}$. The state of the system is known at the center of the calculation cells and it is defined by the cell-averaged values $\tilde{\bar{h}}_{i;j}$ and $\tilde{\bar{v}}_{i;j}^{l}$.

In this paper, the time integration of equations (8) and (9) is carried out by means of a third order accurate Strong Stability Preserving Runge-Kutta method (SSPRK) reported in [11]. The SSPRK method can be written in compact form as follows

$$\tilde{\bar{h}}_{i;j}^{(0)} = \tilde{\bar{h}}_{i;j}^{(n)} \quad ; \quad \tilde{\bar{v}}^{l}{}_{i;j}^{(0)} = \tilde{\bar{v}}^{l}{}_{i;j}^{(n)} \qquad (10)$$

$$\tilde{\bar{h}}_{i;j}^{(p)} = \sum_{q=0}^{p-1}\left[\Omega_{pq} h_{i,j}^{(q)} + \Delta t\varphi_{pq}\boldsymbol{L}\left(v^{1(q)}, v^{2(q)}\right)\right] \qquad (11)$$

$$\tilde{\bar{v}}^{l}{}_{i;j}^{(p)} = \sum_{q=0}^{p-1}\left[\Omega_{pq}\tilde{\bar{v}}^{l}{}_{i;j}^{(q)} + \Delta t\varphi_{pq}\boldsymbol{D}\left(h^{(q)}, v^{1(q)}, v^{2(q)}\right)\right] \qquad (12)$$

$$\tilde{\bar{h}}_{i;j}^{(n+1)} = \tilde{\bar{h}}_{i;j}^{(3)} \quad ; \quad \tilde{\bar{v}}^{l}{}_{i;j}^{(n+1)} = \tilde{\bar{v}}^{l}{}_{i;j}^{(3)} \qquad (13)$$

where $p = 1,2,3$. See [11] for the Ω_{pq} and φ_{pq} values.

For the calculation of the $\boldsymbol{L}(v^1, v^2)$ and $\boldsymbol{D}(h,\ v^1, v^2)$ terms, the numerical approximation of integrals on the right-hand side of equations (6) and (7) is required. This calculation is based on the following sequence

1. Starting from cell averaged values, the point values of the unknown variables at the centre of the contour segments which define the calculation cells are computed by means of WENO reconstructions. Two WENO reconstructions defined on two adjacent cells are used to get two point values of the unknown variables at the centre of the contour segment which is common with the two adjacent cells.

2. The point values of the unknown variables at the centre of the contour segments are advanced in time by means of the so-called exact solution of a local Riemann problem, with initial data given by the pair of point-values computed by two WENO reconstructions defined on the two adjacent cells. In accordance with the procedure proposed by [9], all Riemann problems are solved in a locally valid orthonormal basis. This orthonormalization allows to solve Cartesian Riemann problems that are devoid of metric terms.

3. The spatial integrals that define the $\boldsymbol{L}(v^1, v^2)$ and $\boldsymbol{D}(h,\ v^1, v^2)$ terms are numerically approximated by means of a high order quadrature rule, starting from point values of the dependent variables computed at the previous step.

3.1 The WENO reconstructions

The WENO reconstructions of the point values of the free surface elevation η are here reported. Let us indicate by $(\overline{\eta})_{i,j}$ the cell averaged values of the free surface elevation η over the cell $I_{i,j}$. We also indicate by $(\eta)_{i+1/2,j}$ and $(\eta)_{i-1/2,j}$, respectively,

the two point values of η at the center of the segments over which the coordinate ξ^1 is constant and that are placed on the side of increasing and decreasing ξ^1. For the sake of brevity, we will only present the reconstruction technique of these point values. Two different steps are involved in this reconstruction:

- step 1: reconstruction of the line average values $(\tilde{\eta})_{i,j}$ along the coordinate ξ^2, starting from the cell average values $(\overline{\eta})_{i,j}$

$$(\tilde{\eta})_{i,j} = \frac{1}{\Delta\xi^1}\int_{\xi^1_{i-1/2,j}}^{\xi^1_{i-1/2,j}} \eta(\xi^1,\xi^2)d\xi^1 \qquad (14)$$

- step 2: reconstruction of the point values $(\eta)_{i+1/2,j}$ and $(\eta)_{i-1/2,j}$ along the coordinate ξ^2, starting from the line average values $(\tilde{\eta})_{i,j}$.

1) Step 1

The value of $(\tilde{\eta})_{i,j}$ is reconstructed by using an interpolant polynomial $R_{i,j}(\xi^2)$ which is defined in the cell $I_{i,j}$ and by using the relation $(\tilde{\eta})_{i,j} = R_{i,j}(\xi^2_j)$. According to the formulation of the WENO schemes in the work of [7], the polynomial $R_{i,j}(\xi^2)$ is given by a convex combination of three different 2nd order polynomials, $P_{i,j+p}(\xi^2) = a_{i,j+p}(\xi^2)^2 + b_{i,j+p}(\xi^2) + c_{i,j+p}$ with $p = -1,0,1$. The weights of this convex combination are a function of the linear weights and the indexes of smoothness [6]. As suggested in [6], the norm L^2 of the derivatives of the polynomials $P_{i,j+p}(\xi^2)$ on cell $I_{i,j}$ is used in order to compute the indexes of smoothness. The linear weights are chosen in such a way that the required accuracy is satisfied. The Jacobian terms may affect the weights evaluated in the WENO reconstruction procedure, even when imposing the free stream value. As suggested in [8], the Jacobian terms are not included in the reconstruction procedures and, therefore, the cell averaged value is approximated by

$$(\overline{\eta})_{i,j+p+q} = \frac{1}{\Delta\xi^2} \int_{\xi^2_{i,j+p+q-1/2}}^{\xi^2_{i,j+p+q+1/2}} \left[\frac{1}{\Delta\xi^1}\int_{\xi^1_{i-\frac{1}{2},j+p}}^{\xi^1_{i+\frac{1}{2},j+p}} \eta(\xi^1,\xi^2)d\xi^1\right] d\xi^2 \qquad (15)$$

By imposing

$$P_{i,j+p}(\xi^2) = \frac{1}{\Delta\xi^1}\int_{\xi^1_{i-\frac{1}{2},j+p}}^{\xi^1_{i+\frac{1}{2},j+p}} \eta(\xi^1,\xi^2)d\xi^1 \qquad (16)$$

and by introducing (16) into (15), the above condition becomes

$$(\overline{\eta})_{i,j+p+q} = \frac{1}{\Delta\xi^2}\int_{\xi^2_{i,j+p+q-1/2}}^{\xi^2_{i,j+p+q+1/2}} \left[P_{i,j+p}(\xi^2)\right] d\xi^2 \qquad (17)$$

By introducing the analytical solution of the integral in (17), three independent systems are obtained ($p = -1,0,1$), each of them is formed by three linear equations ($q = -1,0,1$), which permit the computation of the values of the polynomial coefficients $a_{i,j+p}$, $b_{i,j+p}$, $c_{i,j+p}$. Starting from these values and the values of the smoothness indexes, it is possible to calculate $R_{i,j}(\xi^2)$ and, consequently, to evaluate $(\tilde{\eta})_{i,j}$.

2) Step 2

In the second step, the passages shown in the first step are carried out along the coordinate ξ^1. Starting from the line average values $(\tilde{\eta})_{i,j}$, the two point values of the free surface elevation at the centre of the faces over which the coordinate ξ^1 is constant and that are placed on the side of increasing and decreasing ξ^1 are computed by

$$(\eta)_{i+1/2,j} = R_{i,j}(\xi^1_{i+1/2})\ ;\ (\eta)_{i-1/2,j} = R_{i,j}(\xi^1_{i-1/2}) \qquad (18)$$

3.2 The wet and dry advancing solution

In the numerical integration of the equations of motion (6) and (7) a particular treatment of the advancing solution of the shallow water equations on dry bed (wet and dry front) is requested. In order to simulate the wet and dry front, the following original procedure is proposed.

For the sake of brevity the procedure of the wet and dry front is exposed referenced to a line which is parallel to the curvilinear coordinate line ξ^2. At the centre of the segments which separate the dry cell $I_{i;j}$ from the wet cell $I_{i-1;j}$, point values of the unknown variables are reconstructed, by means of an asymmetric WENO reconstruction defined on the wet cell. For example, at the centre of the segment which is the interface between dry cell $I_{i;j}$ and wet cell $I_{i-1;j}$, WENO reconstructions defined on the $I_{i-1;j}$ cell lead to the evaluation of the variables $h^{(n)-}_{i-1/2;j}$ and $v^{l\,(n)-}_{i-1/2;j}$. The advancing in time is carried out by means of the exact solution of an apposite Riemann problem, with initial data given by the pair of point-values computed by the WENO reconstruction. It must be noted that the point values

of the unknown variables $h_{i-1/2;j}^{(n)+}$ and $v^{l}{}_{i-1/2;j}^{(n)+}$ are equal to zero because they belong to the dry cell $I_{i;j}$.

Let us define $\rho^{1(n)}$ and $\tau^{1(n)}$ as the depth-averaged components that are respectively normal and tangential to the coordinate line ξ^2. By defining $\vec{g}^{(1)}/\sqrt{g^{11}}$ and $\vec{g}_{(2)}/\sqrt{g_{22}}$ as the unit vectors which are respectively normal and tangential to the coordinate line ξ^2 and by recalling the transformation relationships, eq. (1), the following transformation relations are obtained

$$\rho^{1(n)} = \frac{v^{1(n)}}{h\sqrt{g^{11}}} \tag{19}$$

$$\tau^{1(n)} = \frac{v^{1(n)}}{h}\frac{g_{12}}{\sqrt{g_{22}}} + \frac{v^{2(n)}}{h}\sqrt{g_{22}} \tag{20}$$

For example, in the point of coordinates $\left(\xi_{i-1/2}^{1}, \xi_{j}^{2}\right)$ belonging to the segment that lies on the coordinate line ξ^2, which is the interface of cells $I_{i-1;j}$ and $I_{i;j}$, the WENO reconstruction lead to the definition of the point values of dependent variables $h_{i-1/2;j}^{(n)-}$, $\rho^{1}{}_{i-1/2;j}^{(n)-}$ and $\tau^{1}{}_{i-1/2;j}^{(n)-}$.

Let define as $h_{i-1/2;j}^{(n+1)^*}$, $\rho^{1}{}_{i-1/2;j}^{(n+1)^*}$ and $\tau^{1}{}_{i-1/2;j}^{(n+1)^*}$ the solution, at the advanced time level t^{n+1}, of the wet and dry Riemann problem defined by the hyperbolic homogeneous system of the shallow water equations, written in the locally valid orthonormal basis, and let $s_{i-1/2;j}^{(n+1)^*}$ be the propagation velocity of the wet and dry front. The exact solution of this Riemann problem on the interface between the wet cell $I_{i-1;j}$ and the dry cell $I_{i;j}$ gives

$$h_{i-1/2;j}^{(n+1)^*} = \frac{1}{G}\left\{\frac{1}{3}\left[\rho^{1}{}_{i-1/2;j}^{(n)-} + 2\left(Gh_{i-1/2;j}^{(n)-}\right)^{\frac{1}{2}}\right]\right\}^{\frac{1}{2}} \tag{21}$$

$$\rho^{1}{}_{i-1/2;j}^{(n+1)^*} = \frac{1}{3}\left[\rho^{1}{}_{i-1/2;j}^{(n)-} + 2\left(Gh_{i-1/2;j}^{(n)-}\right)^{\frac{1}{2}}\right] \tag{22}$$

$$\tau^{1}{}_{i-1/2;j}^{(n+1)^*} = \tau^{1}{}_{i-1/2;j}^{(n)-} \tag{23}$$

$$s_{i-1/2;j}^{(n+1)^*} = \rho^{1}{}_{i-1/2;j}^{(n)-} + 2\left(Gh_{i-1/2;j}^{(n)-}\right)^{\frac{1}{2}} \tag{24}$$

Let $dwd_{i-1/2;j}^{(n+1)}$ be the distance of the wet and dry front to the interface between the wet cell $I_{i-1;j}$ and the dry cell $I_{i;j}$. Such distance is given by

$$dwd_{i-1/2;j}^{(n+1)} = dwd_{i-1/2;j}^{(n)} + \left[\rho^{1}{}_{i-1/2;j}^{(n)-} + 2\left(Gh_{i-1/2;j}^{(n)-}\right)^{\frac{1}{2}}\right]\Delta n \tag{25}$$

where Δn is the time step. Finally, by an inverse transformation of the reference system, the solution of the Riemann problem in the curvilinear coordinate system is evaluated.

4 Model validation

The proposed model is tested in the classical flat-bed dam-break problem. Two regions are separated at x =0m by a wall. In the left region still water level of initial depth h_0 is present, while the right region is dry. The evolution of this initial conditions after the removal of the wall, and consequently the release of the water, is numerically simulated.

The solution of the classical flat-bed dam-break generated by the instantaneous removal of the wall at time t =0 is given by the Ritter solution [12] as

$$h^* = \frac{1}{9}\left(2 - \frac{x^*}{t^*}\right)^2 \tag{26}$$

$$u^* = \frac{2}{3}\left(\frac{x^*}{t^*} + 1\right) \tag{27}$$

where h^* and u^* are respectively the dimensionless water depth and the fluid velocity.

The analytical solution valid for h_0^* =1 is represented in Figure 1 (solid line) at different dimensionless times $t^* = 0.00$, 0.07, 0.12 and 0.20. The numerical results obtained by the presented high-order WENO reconstruction numerical model are shown in the same figure (points). The numerical results obtained by numerically simulating the classical dam-break problem are in very good agreement with the analytical solution.

The flat-bed dam-break test is particularly suitable to test the shock-capturing properties of the solver, highlighting any possible weakness. In fact, this test makes it possible to see that the choice of the order of accuracy of the numerical scheme is critical when simulating the wet and dry phenomenon.

Figure 2 shows the comparison between the analytical solution (solid line) and the solution obtained by adopting a first order accurate numerical scheme (points) at different dimensionless times. By observing Figure 2 it is possible to see that these numerical results significantly differ from the analytical solution.

By comparing the first-order accurate solution (Figure 2) with the solution obtained by adopting the high-order accurate WENO scheme (Figure 1) it is possible to deduce that the shock-capturing properties of the model are strictly related to the choice of the accuracy order of the numerical scheme.

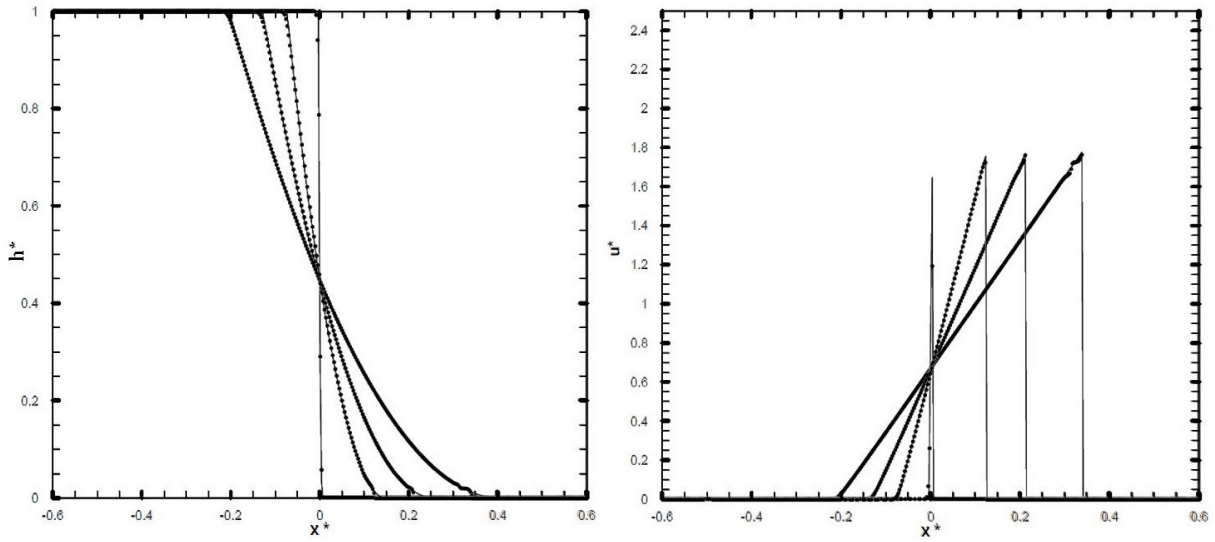

Fig. 1: Flat-bed dam-break problem. Comparison between the analytical solution (solid lines) and numerical results obtained with the high-order WENO scheme (points) in terms of dimensionless water depth, h^*, and dimensionless fluid velocity, u^*, at different dimensionless times $t^* = 0.00, 0.07, 0.12, 0.20$.

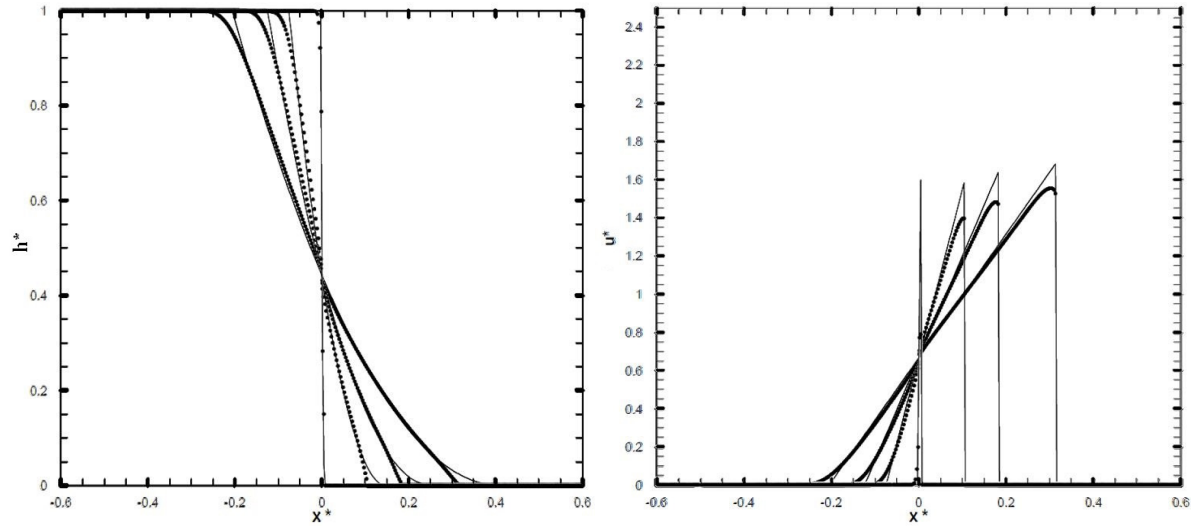

Fig. 2: Flat-bed dam-break problem. Comparison between the analytical solution (solid lines) and numerical results obtained with the first-order accurate numerical scheme (points) in terms of dimensionless water depth, h^*, and dimensionless fluid velocity, u^*, at different dimensionless times $t^* = 0.00, 0.07, 0.12, 0.20$.

5 Rio Fucino dam-break simulation

The proposed model is used to simulate the shock wave caused by the instantaneous Rio Fucino dam-break. Table 1 shows the significant data of the dam and of the reservoir as reported by the Operating Conditions and Maintenance Template of the dam operator.

Table 1: Rio Fucino dam and Campotosto reservoir significant data as reported by the Operating Conditions and Maintenance Template

Maximum height	49m
Full supply level	39m
Crest length	154m
Capacity	$218 \cdot 10^6 m^3$

The simulation of the shock wave generated by the instantaneous Rio Fucino dam-break has been carried out in the case in which the initial level coincides with the full supply level (see Table 1).

The computational domain reproduces a wide area including the Campotosto reservoir and a segment of the Rio Fucino River that stretches out over 23.5km downstream the dam. At the end of such segment (last 2.3km), the width of the computational domain settles to around 1km, in such a way to include the areas occupied by the buildings included in the town of Montorio al Vomano. At the upstream boundary of the computational domain a flow closed boundary condition has been adopted, while at the downstream boundary of the computational domain a zero gradient boundary condition is applied once the shock-wave front has reached the boundary. The above simulation is performed using a curvilinear grid which is made up of 25843cells. Figure 3 shows a detail of such curvilinear grid which includes the Campotosto reservoir and the Rio Fucino dam. The Manning's coefficient is set to $0.05 m^{-1/3}$ and the Courant number is set equal to 0.25.

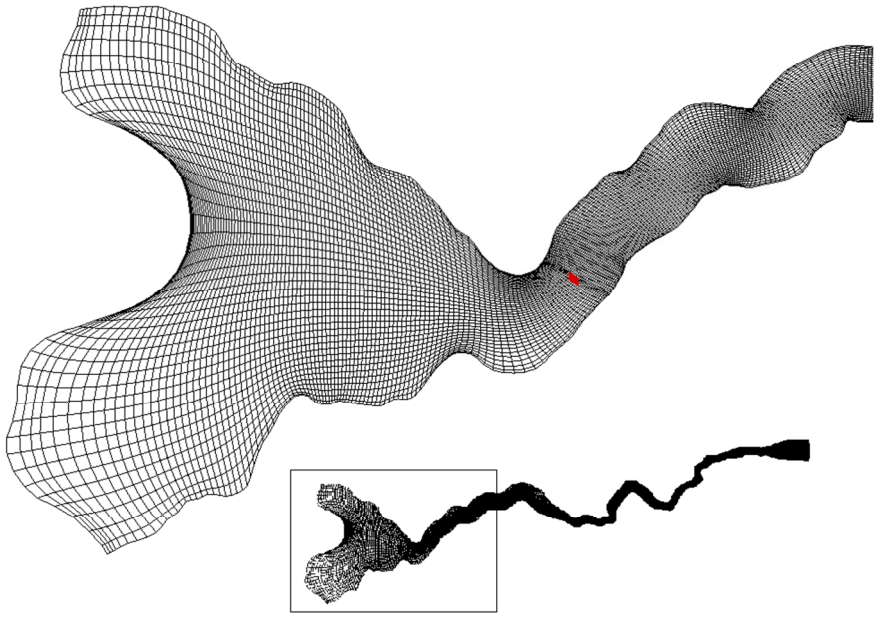

Fig. 3: Curvilinear calculation grid detail. Campotosto reservoir and Rio Fucino dam.

In Figure 4 a detail of the calculation curvilinear grid showing the Rio Fucino dam is presented. In the same figure, the collapse of the dam and the following water flood is shown. The Rio Fucino dam-break causes the spillage of about $31.000 m^3$ of water.

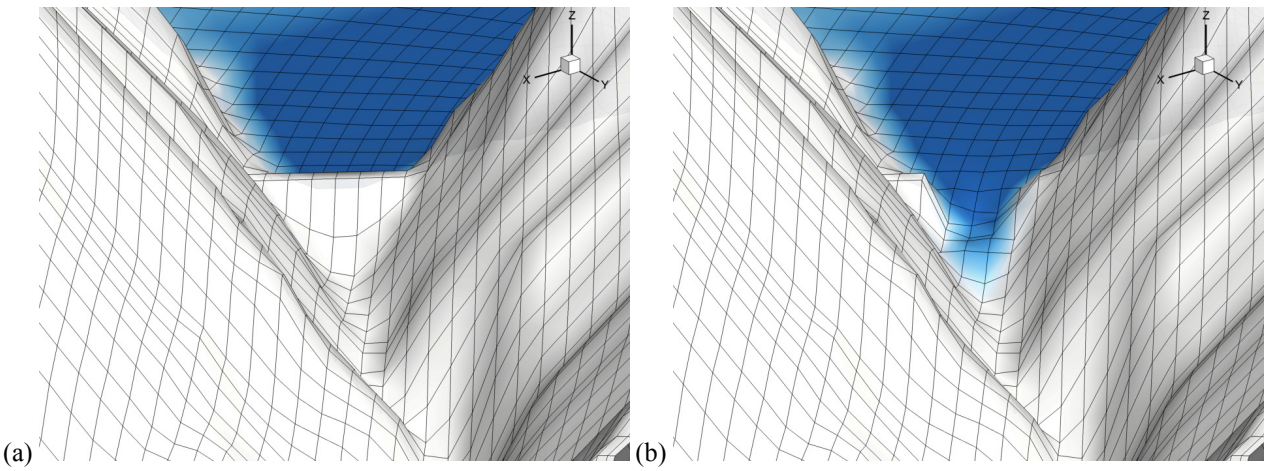

(a) (b)

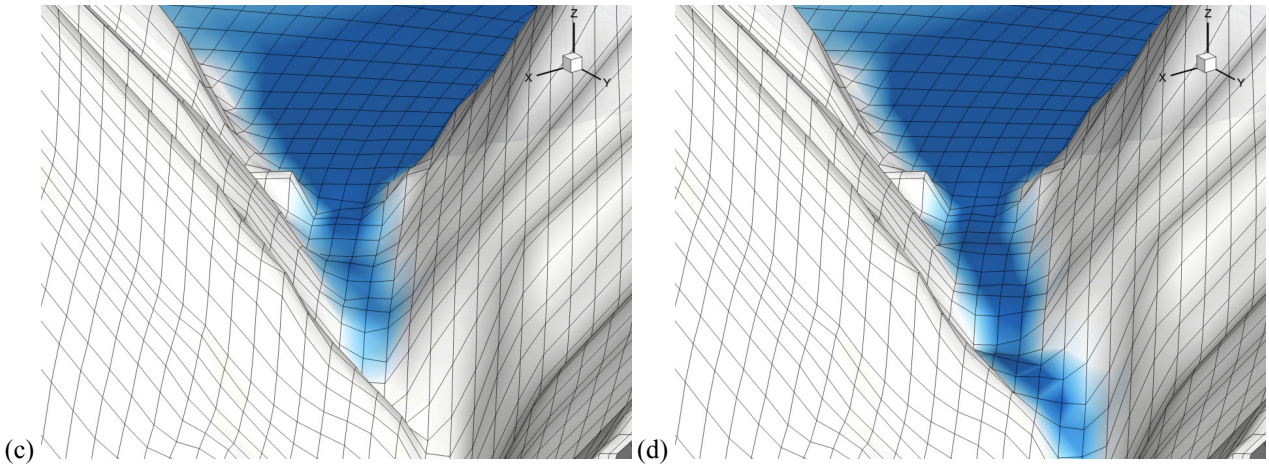

Fig. 4: (a) Curvilinear calculation grid detail showing the Rio Fucino dam at t=0s. Spreading of the shock wave front over the Vomano River after the dam failure at (b) t=7.5s, (c) t=30s, (d) t=60s

The numerical results allow us to deduce that the shock wave generated as the result of the instantaneous Rio Fucino dam-break spreads rapidly in the stretch of river downstream of the dam, reaching considerable heights in correspondence to the houses belonging to the Montorio al Vomano municipality. In fact, the time taken by the wave front to reach the first houses (about 21km from the dam) is about 66minutes and, once these have been hit by the shock wave, the maximum water height is about 15m. Figure 5 shows the spreading of the wave front over the Vomano valley after the dam failure. Figure 5 shows how the presented model is able to simulate the advancing of the wave front and the evolution of the boundaries of the wet area over the complex geometries of the stretch of river downstream the Rio Fucino dam. In particular, by observing Figure 5 it is also possible to notice the high degree of irregularity of the computational domain corresponding to the sharp bends of the river in the area that precedes the considered final section.

In Figure 6 a detail of the spreading of the wave front over the Vomano valley after the dam failure at the Montorio al Vomano municipality is shown at different times. In this area, the Vomano River valley floor expands, from a deep valley with steep banks, to shallower slopes and broader and gentler area.

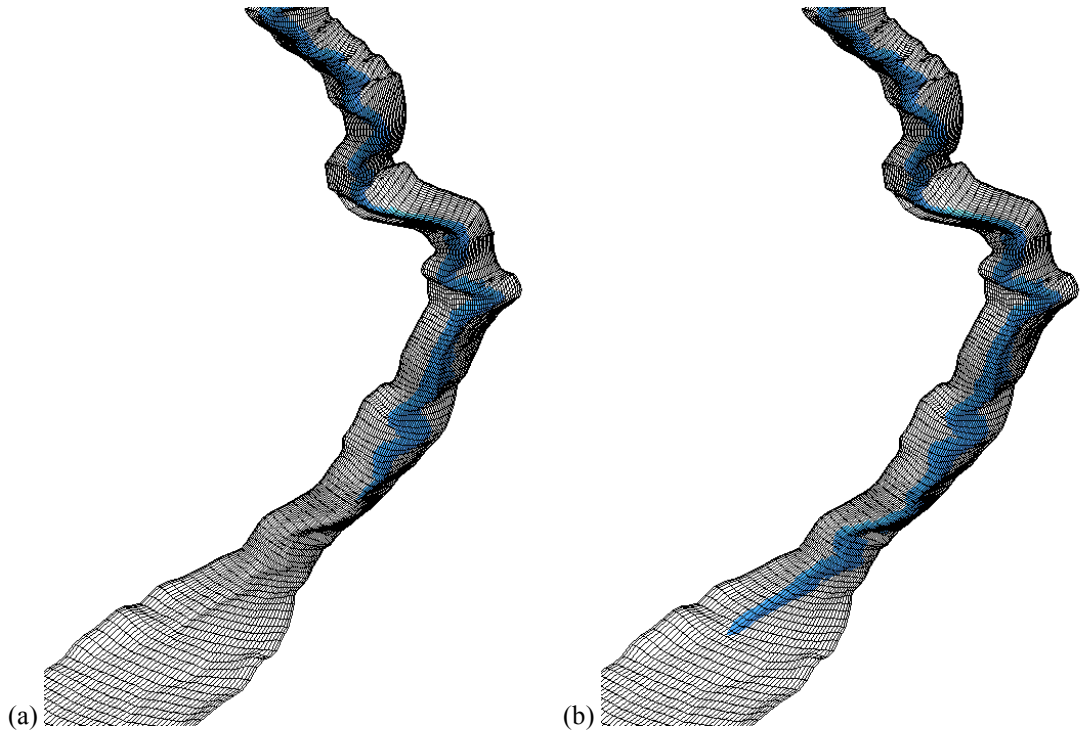

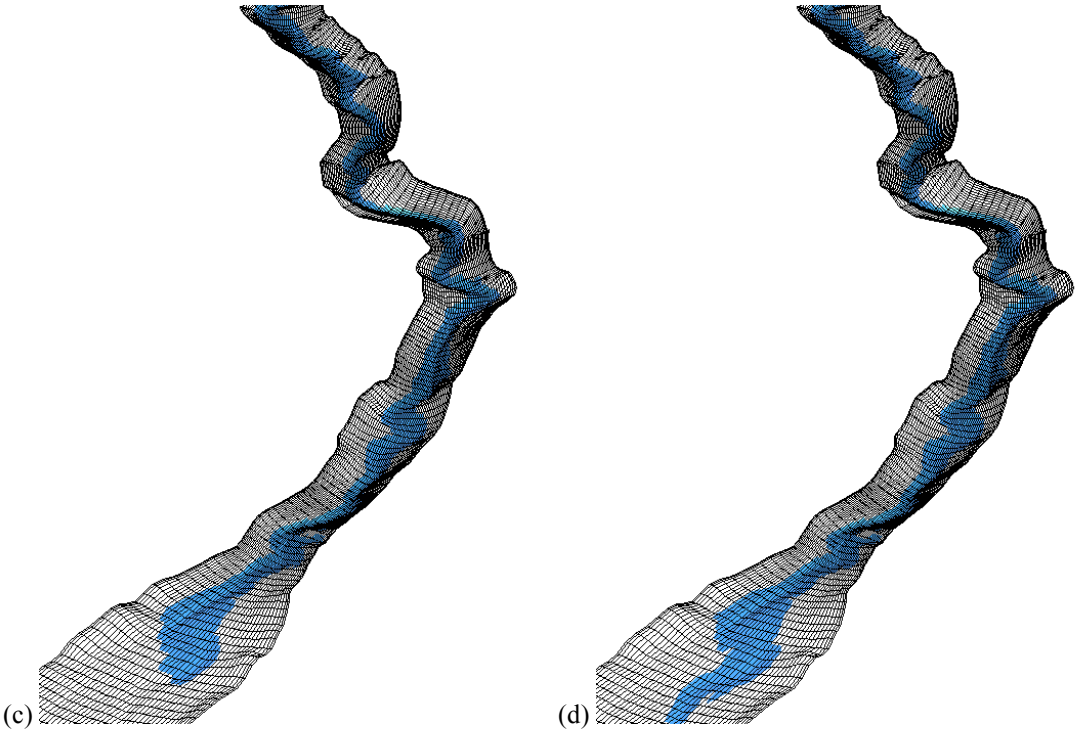

Fig. 5: Spreading of the shock wave front over the Vomano River valley floor after the dam failure. Instantaneous elevation of the shock wave at (a) t=62.5min, (b) t=68.5min, (c) t=71.25min, (d) t=73.75min

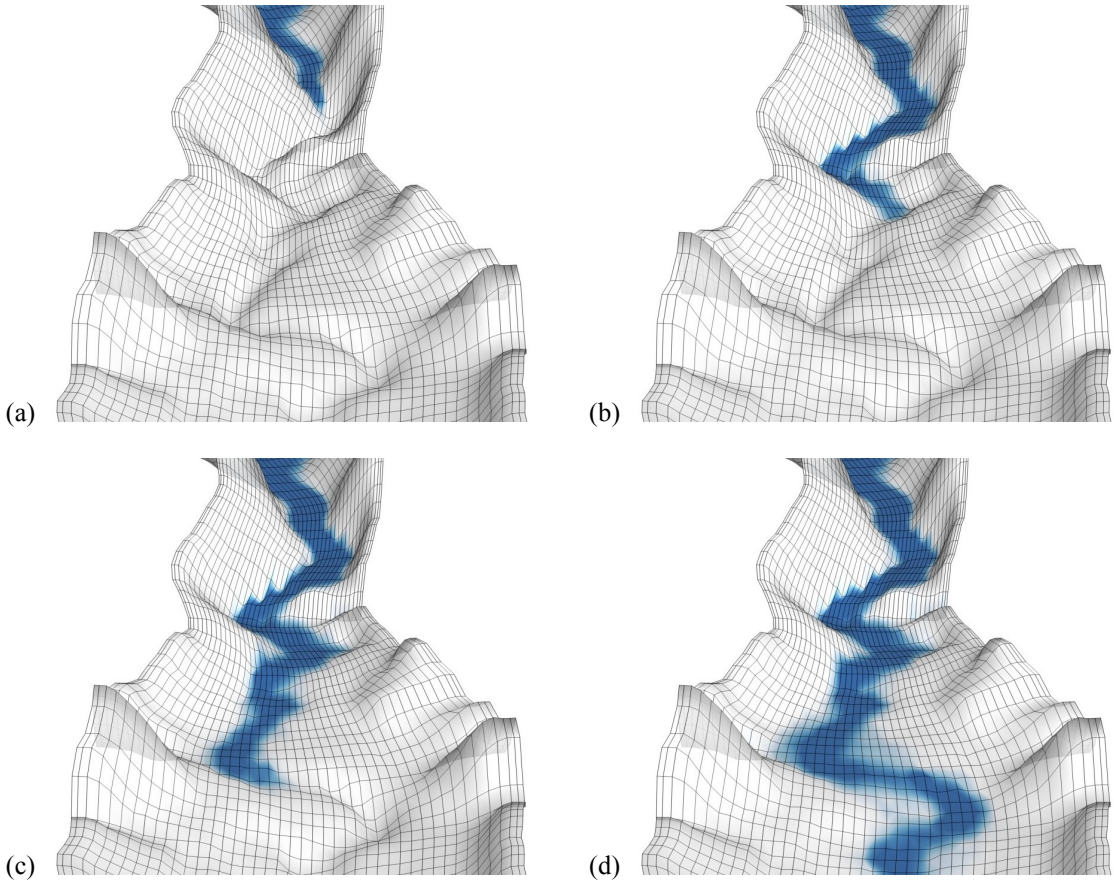

Fig. 6: Detail of the spreading of the shock wave front over the Vomano River valley floor after the dam failure. Instantaneous elevation of the shock wave at (a) t=62.5min, (b) t=64.5min, (c) t=67.5min, (d) t=73min

The numerical results have been used in order to realize the flood map downstream of the Rio Fucino dam (Figure 7) corresponding to the dam-break and subsequent emptying of the Campotosto reservoir, in the case of initial full supply water level. By observing Figure 7 it can be deduced that, for a full supply water level, the dam-break would lead to the flooding of a considerable portion of the Montorio al Vomano municipality.

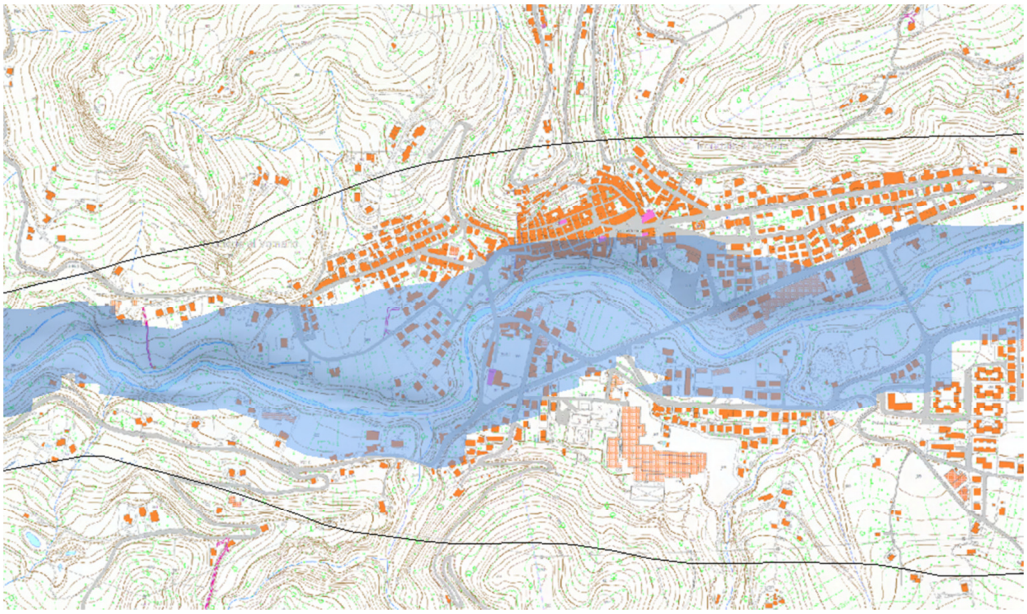

Fig. 7: Detail of the flood map downstream of the Rio Fucino dam over the Vomano River valley floor

6 Conclusion

A dam-break flood model based on a contravariant integral form of the shallow water equations has been presented. This model is used in order to simulate the dam-break phenomenon over computational domains characterized by complex shapes, in which the advancing in time of the flood wave front is carried out by means of an original wet and dry scheme. It has been demonstrate that the model correctly simulates the wet front progress velocity. The presented model is used to simulate the shock (flood) wave caused by the instantaneous Rio Fucino dam-break. The simulation results make it possible to deduce that the shock wave reaches considerable water heights in correspondence to the houses belonging to the Montorio al Vomano municipality.

References:

[1] Aris, R., *Vectors, tensors, and the basic equations of fluid mechanics*, New York, USA, Dover, 1989.

[2] Cannata, G., Lasaponara, F. & Gallerano, F., Non-Linear Shallow Water Equations numerical integration on curvilinear boundary-conforming grids, *WSEAS Transactions on Fluid Mechanics*, No. 10, 2015, pp. 13-25.

[3] Gallerano, F., Cannata, G. & Lasaponara, F., Numerical simulation of wave transformation, breaking run-up by a contravariant fully nonlinear Boussinesq model, *Journal of Hydrodynamics B*, No. 28, 2016, pp. 379-388.

[4] Gallerano, F., Cannata, G. & Lasaponara, F., A new numerical model for simulations of wave transformation, breaking and long shore currents in complex coastal regions, *International Journal for Numerical Methods in Fluids*, No. 80, 2016, pp. 571-613.

[5] Gallerano, F., Cannata, G. & Tamburrino, M., Upwind WENO scheme for shallow water equations in contravariant formulation, *Computers & Fluids*, No. 62, 2012, pp. 1-12.

[6] Jiang, G. S. & Shu, C. W., Efficient implementation of weighted ENO schemes, *Journal of Computational Physics*, No. 126, 1996, pp. 202-228.

[7] Liu, X., Osher, S. & Chan, T., Weighted essentially non-oscillatory schemes. *Journal of Computational Physics*, No. 115(1), 1994, pp. 200-212.

[8] Nonomura, T., Iizuka, N. & Fujii, K., Free stream and vortex preservation properties of high-order WENO and WCNS on curvilinear grids, *Computers & Fluids*, No. 39, 2010, pp. 197-214.

[9] Rossmanith, J.A., Bale, D.S. & LeVeque, R.J., A wave propagation algorithm for hyperbolic systems on curved manifolds, *Journal of Computational Physics*, No. 199(2), 2004, pp. 631-662.

[10] Shi, F., Kirby, J.T., Harris, J.C., Geiman, J.D. & Grilli, S.T., A high-order adaptive time-stepping TVD solver for Boussinesq modeling of breaking waves and coastal inundation. *Coastal Engineering*, No. 193(1), 1998, pp. 90-124.

[11] Spiteri, R.J. & Ruuth, S.J., A new class of optimal high-order strong stability-preserving time discretization methods, *SIAM Journal on Numerical Analysis*, No. 40(2), 2002, pp. 469-491.

[12] Stoker, J. J., *Water Waves*, Interscience: New York, 1957.

[13] Tonelli, M. & Petti, M., Hybrid finite-volume finite-difference scheme for 2HD improved Boussinesq equations. *Coastal Engineering*, No. 56, 2009, pp. 609-620.

[14] Toro, E., *Shock-capturing methods for free-surface shallow flows*, John Wiley and Sons: Manchester, 2001.

[15] Valiani, A., Caleffi, V. & Zanni, A., Case study: Malpasset dam-break simulation using a two-dimensional finite volume method, *Journal of Hydraulic Engineering*, No. 128, 2002, pp. 460-472.

[16] Xing, Y. & Shu, C.W., High order well-balanced finite volume WENO schemes and discontinuous Galerkin methods for a class of hyperbolic systems with source terms, *Journal of Computational Physics*, No. 214(2), 2006, pp. 567-598.